Using UTE images for bone/air segmentation: applications for radiation therapy

Weili Zheng[1], Joshua P. Kim[1], Indrin J. Chetty[1], and Carri K. Glide-Hurst[1]

[1]*Radiation Oncology, Henry Ford Health System, Detroit, Michigan, United States*

TARGET AUDIENCE

Researchers and clinicians interested in *ultrashort echo time* (UTE) imaging, MRI applications in radiation therapy, and attenuation corrections for PET/MRI.

PURPOSE

Accurate bone segmentation is essential for the generation of (i) electron density maps needed for dose calculation in MR-only radiotherapy treatment planning (RTP) and (ii) MR-based attenuation correction maps in hybrid PET/MRI systems. While UTE sequences improve the visualization of tissues with short T2 such as cortical bone (1), efficient and robust segmentation of bone and air remains a significant challenge (2). To address this need, we introduce an application that uses a novel hybrid magnitude and phase UTE approach to differentiate tissue types, facilitate accurate segmentation, and generate synthetic CTs (synCTs) for the brain.

MATERIALS AND METHODS

Data acquisition: Brain scans of five healthy volunteers and eight brain cancer patients were acquired on a Philips 1.0T Panorama High Field Open system using an 8 channel head coil. T1-W, T2-TSE and FLAIR images were acquired in the same field of view with the following parameters. T1-W: TR/TE/α=25/6.9ms/30°, voxel size 0.96/0.96/2.5mm; T2-TSE:TR/TE/α =3802/80ms/90°, voxel size 0.68/0.68/2.5mm; FLAIR: TR/TI/TE/α =11000/ 2800/140ms/90°, voxel size 0.9/0.9/3mm. A novel sequence combining UTE-DIXON datasets and magnitude and phase images were collected using 3D radial acquisition at echo times of either $TE_1/TE_2/TE_3$ =0.14/2.44/4.74 ms or $TE_1/TE_2/TE_3$ =0.14/3.54/6.94 ms, α =25°, TR=11.5 ms , 1.2~1.3mm isotropic voxel reconstructed to 0.96~1mm, with acquisition times of approximately 9mins.

Image processing: Images are processed through the workflow shown in Fig.1. **(Step 1: Bone enhancement (Dashed region in Fig. 1))** An inverted UTE magnitude image was generated from the first echo (TE1) by using the maximum intensity of the magnitude image (Fig. 2a) minus the image itself. Water/fat maps were reconstructed using a conventional 2-point Dixon method. An optimal weighted combination of inverted UTE (Fig. 2b) and water/fat maps resulted in a bone-enhanced image (Fig. 2c). **(Step 2: Air Segmentation (Solid region in Fig. 1))** Original phase images (Fig.2d) at TE1 were unwrapped using a 3D phase unwrapping algorithm (3). The head mask applied before unwrapping was generated via thresholding the magnitude image. The susceptibility induced, chemical shift related phase and phase zero map were obtained by solving the equations from three echoes based the three components phase model (4). A Gaussian Mixture Model (GMM) classifier was then applied to the phase zero map (Fig. 2e) to segment air from tissues and bones (part of the cerebral spinal fluid (CSF) included). To further remove CSF from air, T2-TSE images were co-registered to the phase image, CSF was segmented using a GMM model and a corrected air-only mask was generated. This air mask was applied to the bone-enhanced image (Fig. 2c) resulting in a final bone-enhanced image with air labeled as zero (Fig. 2f). **(Step 3: SynCT)** Previously, synCTs were developed by our group using manual segmentation of bones combined with a voxel-based weighted summation of T1-W, T2-W and FLAIR datasets for pelvis (5). This synCT workflow was modified for brain by incorporating the bone-enhanced images and air masks along with the T1-W, T2-W, and FLAIR datasets to generate synCTs and results were compared with patient CTs.

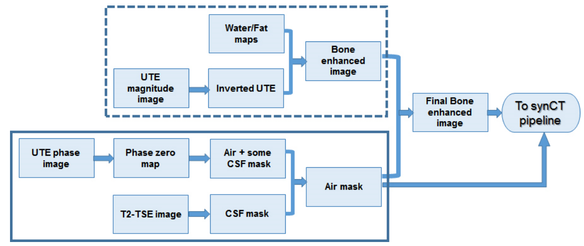

Fig. 1 Image processing workflow. Dashed line shows the bone enhancement processing steps while solid boundary outlines the air segmentation steps.

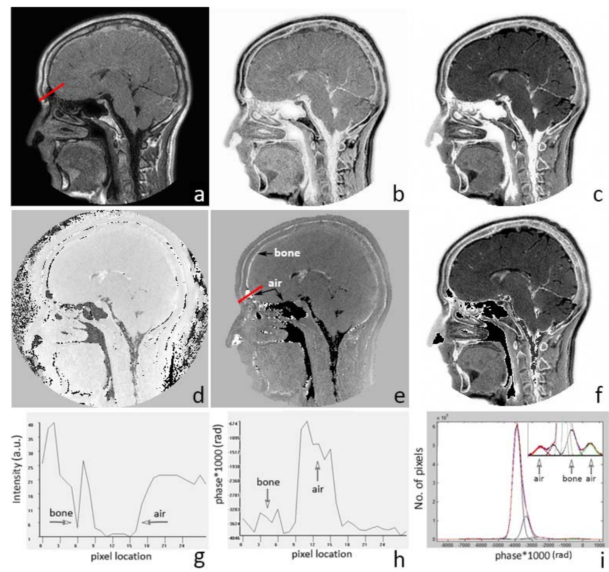

Fig. 2 (a) UTE magnitude at TE=0.144ms; (b) inverted UTE magnitude image; (c) bone enhanced image; (d) original UTE phase; (e) phase zero map; (f) final bone enhanced image; (g) signal intensity profile and (h) phase value profile along the red lines marked in (a) & (e), respectively; (i) histogram of zero phase and the fitting of a GMM model with 6 kernels indicating air and bone.

RESULTS The inverted UTE magnitude image highlighted bone out of the other tissue types (Fig. 2b). After weighted combination with water/fat maps, the bone/brain contrast (= (bone intensity-brain tissue intensity)/ brain tissue intensity) was increased from 0.1 (Fig. 2b) to 2.5 (Fig. 2c). In the original phase image (Fig. 2d), air and CSF around the spinal cord (due to the off-resonance effect) had signal void. These signal void regions became extremely bright or dark after phase unwrapping (Fig. 2e). Thus they were easily identified in the intensity histogram (Fig. 2i) as the Gaussian kernels with lowest and highest means in the expectation-maximization fitting of a 6-kernel GMM model. Though the UTE magnitude image (Fig. 1a) yielded measurable signal intensity at 0.144 ms, the line intensity profiles (Fig. 2g&h) illustrated that air/bone contrast in the zero phase map was substantially larger and thus more favorable for air segmentation. The mask (air+CSF) generated from the GMM classifier was compared with the CSF mask obtained from the T2 image resulting in a desired air mask. Fig 3 illustrates several slices of synCT compared to CT for a brain cancer patient, showing that the bony skull and air cavities (sinus and ear canals) agreed well between datasets.

CONCLUSION We have introduced a hybrid phase/magnitude UTE image processing technique, that when combined with standard MRI images, significantly improved bone and air contrast in MRI for more accurate image segmentation. Air masks and post-processed images (i.e. inverted UTE magnitude and bone-enhanced images) were integrated into our synCT pipeline for the brain and results agreed well with clinical CTs. The generation of accurate synCTs is a first step toward MR-only RTP for the brain and essential for future PET/MRI applications.

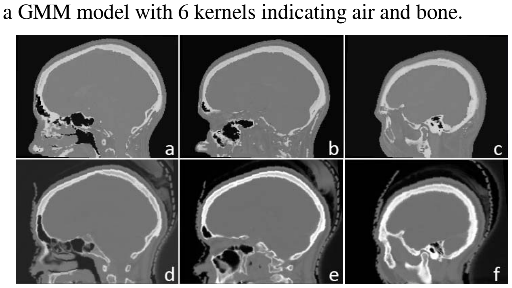

Fig. 3 SynCT (a-c) and treatment planning CT (d-f) of patient data highlighting the close agreement of bone and air visualization between image types.

REFERENCES: (1) Gatehouse PD and Bydder GM, 2003. *Clin Radiol*. 58:1-19. (2) Nyholm T and Jonsson J, 2014, *Semin Radiat Oncol* 24:175-180. (3) Abdul-Rahman HS et al. 2007, Appl Opt. 46:6623-35. (4) Carl M and Chiang J-TA, 2012. *Magn Reson Med*. 67:991-1003. (5) Kim J, et al. 2014, *in Press*, Int J Radiat Oncol Biol Phys.